Detection and characterization of carbon contamination on EUV multilayer mirrors

Juequan Chen[1,*], Eric Louis[1], Chris J. Lee[1,2], Herbert Wormeester[2], Reinhard Kunze[3], Hagen Schmidt[3], Dieter Schneider[4], Roel Moors[5], Willem van Schaik[5], Monika Lubomska[5] and Fred Bijkerk[1,2]

[1]*FOM-Institute for Plasma Physics Rijnhuizen, Nieuwegein, The Netherlands*
[2]*MESA + Research Institute for Nanotechnology, University of Twente, The Netherlands*
[3]*Leibniz Institute for Solid State and Materials Research Dresden, Germany*
[4]*Fraunhofer Institute for Material and Beam Technology IWS Dresden, Germany*
[5]*ASML, Veldhoven, The Netherlands*
**J.Chen@rijnhuizen.nl*

Abstract: In this paper, we detect and characterize the carbon contamination layers that are formed during the illumination of extreme ultraviolet (EUV) multilayer mirrors. The EUV induced carbon layers were characterized *ex situ* using spectroscopic ellipsometry (SE) and laser generated surface acoustic waves (LG-SAW). We show that both LG-SAW and SE are very sensitive for measuring carbon layers, even in the presence of the highly heterogeneous structure of the multilayer. SE has better overall sensitivity, with a detection limit of 0.2 nm, while LG-SAW has an estimated detection limit of 2 nm. In addition, SE reveals that the optical properties of the EUV induced carbon contamination layer are consistent with the presence of a hydrogenated, polymeric like carbon. On the other hand, LG-SAW reveals that the EUV induced carbon contamination layer has a low Young's modulus (<100 GPa), which means that the layer is mechanically soft. We compare the limits of detection and quantification of the two techniques and discuss their prospective for monitoring carbon contamination build up on EUV optics.

©2009 Optical Society of America

OCIS codes: (120.1880) Detection; (120.2130) Ellipsometry and polarimetry; (120.4530) Optical constants; (310.6860) Thin films, optical properties; (340.7480) X-rays, soft x-rays, extreme ultraviolet (EUV)

References and Links

1. E. Louis, A. E. Yakshin, P. C. Goerts, S. Oestreich, R. Stuik, L. G. M. Edward, M. J. H. Kessels, B. Fred, H. Markus, M. Stefan, M. Michael, S. Detlef, S. Frank, and U. Gerhard, "Progress in Mo/Si multilayer coating technology for EUVL optics," Proc. SPIE **3997**, 406–411 (2000).
2. J. Hollenshead, and L. Klebanoff, "Modeling radiation-induced carbon contamination of extreme ultraviolet optics," J. Vac. Sci. Technol. B **24**(1), 64–82 (2006).
3. K.-J. Boller, R.-P. Haelbich, H. Hogrefe, W. Jark, and C. Kunz, "Investigation of carbon contamination of mirror surfaces exposed to synchrotron radiation," Nucl. Instrum. Methods Phys. Res. **208**(1-3), 273–279 (1983).
4. D. L. Windt, "IMD - Software for modeling the optical properties of multilayer films," Comput. Phys. **12**(4), 360–370 (1998).
5. S. Matsunari, T. Aoki, K. Murakami, Y. Gomei, S. Terashima, H. Takase, M. Tanabe, Y. Watanabe, Y. Kakutani, M. Niibe, and Y. Fukuda, "Carbon deposition on multi-layer mirrors by extreme ultra violet ray irradiation," Proc. SPIE **6517**, 65172X–65178 (2007).
6. G. Kyriakou, D. J. Davis, R. B. Grant, D. J. Watson, A. Keen, M. S. Tikhov, and R. M. Lambert, "Electron impact-assisted carbon film growth on Ru(0001): Implications for next-generation EUV lithography," J. Phys. Chem. C **111**(12), 4491–4494 (2007).
7. N. Koster, B. Mertens, R. Jansen, A. van de Runstraat, F. Stietz, M. Wedowski, H. Meiling, R. Klein, A. Gottwald, F. Scholze, M. Visser, R. Kurt, P. Zalm, E. Louis, and A. Yakshin, "Molecular contamination mitigation in EUVL by environmental control," Microelectron. Eng. **61–62**(1-4), 65–76 (2002).
8. R. W. Collins, D. E. Aspnes, and E. A. Irene, "Spectroscopic ellipsometry", in *Proceedings of the 2nd international conference on spectroscopic ellipsometry*, (Elsevier Science S.A., Lausanne, Switzerland, 1998).
9. J. A. Woollam, C. L. Bungay, L. Yan, D. W. Thompson, and J. N. Hilfiker, "Application of spectroscopic ellipsometry to characterization of optical thin films," Proc. SPIE **4932**, 393–404 (2003).

#111052 - $15.00 USD Received 6 May 2009; revised 7 Sep 2009; accepted 7 Sep 2009; published 9 Sep 2009

10. J. A. Woollam, “Overview of Variable Angle Spectroscopic Ellipsometry (VASE), Part I: Basic Theory and Typical Applications,” Proc. *the 44th SPIE meeting*, (1999).
11. D. J. Blaine, H. Jeff, J. I. Natale, M. H. Craig, E. T. Thomas, and A. W. John, “Recent developments in spectroscopic ellipsometry for in-situ applications,” Proc. SPIE **4449**, 41–57 (2001).
12. B. Johs, “General virtual interface algorithm for in situ spectroscopic ellipsometric data analysis,” Thin Solid Films **455–456**, 632–638 (2004).
13. J. A. Roth, W. S. Williamson, D. H. Chow, G. L. Olson, and B. Johs, “Closed-loop control of resonant tunneling diode barrier thickness using in situ spectroscopic ellipsometry,” J. Vac. Sci. Technol. B **18**(3), 1439–1442 (2000).
14. D. Schneider, and T. Schwarz, “A photoacoustic method for characterising thin films,” Surf. Coat. Tech. **91**(1-2), 136–146 (1997).
15. D. Schneider, T. Schwarz, A. S. Bradford, Q. Shan, and R. J. Dewhurst, “Controlling the quality of thin films by surface acoustic waves,” Ultrasonics **35**(5), 345–356 (1997).
16. E. Louis, H. J. Voorma, N. B. Koster, L. Shmaenok, F. Bijkerk, R. Schlatmann, J. Verhoeven, Y. Y. Platonov, G. E. Vandorssen, and H. A. Padmore, “Enhancement of Reflectivity of Multilayer Mirrors for Soft-X-Ray Projection Lithography by Temperature Optimization and Ion-Bombardment,” Microelectron. Eng. **23**(1-4), 215–218 (1994).
17. K. Bergmann, O. Rosier, R. Lebert, W. Neff, and R. Poprawe, “A multi-kilohertz pinch plasma radiation source for extreme ultraviolet lithography,” Microelectron. Eng. **57–8**, 71–77 (2001).
18. J. Chen, C. J. Lee, E. Louis, F. Bijkerk, R. Kunze, H. Schmidt, D. Schneider, and R. Moors, “Characterization of EUV induced carbon films using laser-generated surface acoustic waves,” Diamond Related Materials **18**(5-8), 768–771 (2009).
19. G. E. Jellison, and F. A. Modine, “Parameterization of the optical functions of amorphous materials in the interband region,” Appl. Phys. Lett. **69**(3), 371–373 (1996).
20. G. E. Jellison, and F. A. Modine, “Erratum: Parameterization of the optical functions of amorphous materials in the interband region,” Appl. Phys. Lett. **69**(14), 2137–2137 (1996).
21. J. Hong, A. Goullet, and G. Turban, “Ellipsometry and Raman study on hydrogenated amorphous carbon (a-C: H) films deposited in a dual ECR-r.f. plasma,” Thin Solid Films **352**(1-2), 41–48 (1999).
22. S. Logothetidis, M. Gioti, S. Lousinian, and S. Fotiadou, “Haemocompatibility studies on carbon-based thin films by ellipsometry,” Thin Solid Films **482**(1-2), 126–132 (2005).
23. J. Budai, and Z. Toth, “Optical phase diagram of amorphous carbon films determined by spectroscopic ellipsometry,” Phys. Status Solidi, C **5**(5), 1223–1226 (2008).
24. M. Gioti, and S. Logothetidis, “Dielectric function, electronic properties and optical constants of amorphous carbon and carbon nitride films,” Diamond Related Materials **12**(3-7), 957–962 (2003).
25. J. Tauc, R. Grigorovici, and A. Vancu, “Optical properties and electronic structure of amorphous germanium,” Phys. Status Solidi **15**(2), 627–637 (1966).
26. C. Tanguy, “Optical dispersion by Wannier excitons,” Phys. Rev. Lett. **75**(22), 4090–4093 (1995).
27. C. Tanguy, “Erratum: Optical dispersion by Wannier excitons (vol 75, pg 4090, 1995),” Phys. Rev. Lett. **76**(4), 716–716 (1996).
28. C. Tanguy, “Analytical expression of the complex dielectric function for the Hulthen potential,” Phys. Rev. B **60**(15), 10660–10663 (1999).
29. C. Tanguy, “Refractive index of direct bandgap semiconductors near the absorption threshold: Influence of excitonic effects,” IEEE J. Quantum Electron. **32**(10), 1746–1751 (1996).
30. H. J. Voorma, E. Louis, N. B. Koster, F. Bijkerk, and E. Spiller, “Characterization of multilayers by Fourier analysis of x-ray reflectivity,” J. Appl. Phys. **81**(9), 6112–6119 (1997).
31. S. Frank, B. Burkhard, G. Brandt, R. Fliegauf, K. Roman, M. Bernd, D. Rost, S. Detlef, M. Veldkamp, J. Weser, U. Gerhard, L. Eric, E. Y. Andrey, O. Sebastian, and B. Fred, “New PTB beamlines for high-accuracy EUV reflectometry at BESSY II,” Proc. SPIE **4146**, 72–82 (2000).

1. Introduction

The semiconductor industry’s desire to create smaller integrated circuit features on semiconductors has been a major driver for the development of lithographic techniques and quality optics for short wavelengths. As a part of this trend, the development of EUV lithography, aimed to operate at 13.5 nm, and its component optics has been a major focus over the last ten years. Bragg reflecting optics, i.e. multilayer mirrors (MLMs) must be used because materials are highly absorbing at short wavelengths. MLMs, constructed from alternating layers of silicon and molybdenum, can reach a 69.5% reflectivity [1]. However, there are about ten such optics in the light collection and imaging train, meaning that the throughput of the system is just a few percent. Under these circumstances it is very important to maximize throughput by eliminating or removing surface contaminants that are deposited within the wafer scanner itself.

Wafer scanners may operate under non-UHV conditions. In case of a background pressure on the order of 10^{-3} mbar, and a residual gas mixture consisting of many different components

including water, oxygen and hydrocarbons, the two main sources of contamination are oxidation and the build up of carbon contamination layers. Water acts as an oxidizer, which will etch away soft surfaces, such as silicon. This is usually prevented by using a heavy metal capping layer that forms a stable oxide layer and prolongs the life of the mirror, albeit with a small reflectivity loss.

Unfortunately, the capping layer does not prevent the build up of carbon contamination, leaving it as the main surface contamination process [2]. Even under relatively good vacuum conditions, carbon contamination has been observed, as evidenced by the examination of synchrotron beam line optics [3]. The extremely high absorption of EUV radiation by carbon makes the contamination layer a serious source of loss of optical throughput. For instance, IMD modeling [4] shows that a 1 nanometer thick layer of pure graphite leads to a 1.4% reduction in relative reflectivity ($\Delta R/R_0$) from a single multilayer optic surface. If such a layer were to form on every reflecting surface, it would consume the full lifetime budget of EUVL scanner optics (typically consisting of ten reflecting surfaces). Clearly, such maintenance shutdowns are undesirable, making it necessary to detect, and characterize contaminants before significant optical absorption is observed so that mirror surfaces may be cleaned *in situ* without opening the vacuum chamber. Therefore, a successful monitoring of the contamination process should have a low detection limit, a high sensitivity, a high accuracy and it should be rapid.

This makes it critical to explore and develop techniques that can, during the integrated circuit fabrication processes, accurately detect and track the development of carbon contamination. Critical to achieving accurate carbon contamination monitoring is understanding what form of carbon is deposited on the multilayer structure. Subsequently, a detection technique that has an optimal response to the carbon layer's characteristics can be chosen.

Several techniques have been shown to be sensitive to surface contamination. X-ray photoelectron spectroscopy (XPS) and Auger electron spectroscopy (AES) [5,6], Auger depth profiling analysis [2,7] have been employed to measure the thickness or concentration of EUV induced carbon contamination films. However, these techniques lack sub-nanometer limits of detection and sensitivities. For XPS, there is an additional difficulty due to the potential binding energy overlap between the contamination and capping layer of mirror. Finally, all of these techniques require substantial amounts of space within the vacuum chamber for the electron detector. It makes them undesirable because of the very compact design of the EUVL tool.

On the other hand, ellipsometry is a non-contact, non-destructive and very sensitive technique that uses polarized light to characterize thin films, surfaces, and material microstructure [8–10]. Spectroscopic ellipsometry (SE) can be used to determine optical constants and layer thickness in multilayer stacks. SE also has the advantage that, in measuring changes in polarization, the instrument is largely immune to the intensity noise of the light source. In contrast, reflectivity measurements must be referenced to the input light intensity, adding an additional source of noise. In addition, *in situ* SE has already been developed and applied in some areas of deposition monitoring and active process control [11,12]. The light source, analyzer and other components can remain outside of the vacuum, meaning that only line-of-sight optical access is required. Furthermore, *in situ* SE has been shown to possess sub-monolayer resolution during deposition processes [13].

The surface mechanical properties are also sensitive to changes to the composition of the surface. Surface acoustic waves (SAW), and in particular, laser generated SAW (LG-SAW) can be used to characterize the mechanical properties of thin films, even when the thickness the layer is much smaller than the SAW wavelength [14]. The propagation of SAW depends on the acoustic properties, such as Young's modulus, Poisson's ratio, density, and thickness of the surface and substrate layers. The remote excitation of the acoustic pulse, via a laser pulse, requires only that optical access to the MLM surface is possible, while detection can be achieved using piezoelectric foils or laser interferometery [15].

#111052 - $15.00 USD Received 6 May 2009; revised 7 Sep 2009; accepted 7 Sep 2009; published 9 Sep 2009
(C) 2009 OSA

In this paper, the EUV induced carbon contamination on MLMs has been characterized *ex situ* by SE and LG-SAW. We investigated the sensitivity of both SE and LG-SAW for two carbon layer morphologies. Although SE has a lower limit of detection, we find that LG-SAW is able to distinguish different phases of carbon more accurately.

2. Methodology

2.1 Carbon layer deposition

Briefly, the MLMs investigated here consist of a capping layer plus 50 bi-layers of Mo and Si, each about 7 nm thick, deposited on the (001) surface of a Si wafer. The thickness of the full multilayer stack is 357 nm. A complete description of a typical MLM structure and its properties can be found elsewhere [16].

The MLMs were exposed to EUV radiation from a xenon-based EUV hollow cathode discharge plasma source [17]. The source emits pulses with a duration of 50-100 ns at a repetition frequency of 270 Hz. The radiation in the 10-18 nm range was selected from the broadband emission by passing the light through a zirconium filter attached to a stainless steel box. The samples were placed in the box to protect them from direct exposure to the discharge products. In addition, each mirror was masked so that only half the surface was illuminated, but no measures were taken to prevent hydrocarbons from diffusing under the mask and adsorbing to the surface. The distance between the source and mirror was about 50 cm. Each mirror was evenly illuminated by the filtered EUV light at an energy density of 1.9 $\mu J/cm^2$ per pulse, which is sufficiently low to prevent the mirror from heating significantly over the entire exposure time. Four mirrors were exposed to 0.6 million (~0.6 hour exposure time), 2 million (~2 hour exposure time), 4 million (~4 hour exposure time), and 5 million (~5 hour exposure time) pulses, respectively to obtain four different carbon layer thicknesses.

The residual hydrocarbon gases in the chamber act as the source for the carbon layer deposition. The vacuum in the chamber was between 10^{-6} and 10^{-7} mbar, which increased to 10^{-3} mbar while the EUV source was operating, however, this increase is mainly due to additional xenon. From the residual gas analyzer (RGA) spectrum, a hydrocarbon peak can be easily discriminated from the background. The RGA spectrum showed masses between 62 and 70 mass numbers, which corresponds to Xe^{2+} and background hydrocarbons around the size of pentane or larger.

For the purposes of comparison, additional pairs of MLMs had an amorphous carbon layer deposited on their surfaces by evaporating a graphite filament in close proximity to the MLM surface in a vacuum (which we refer to as "hot filament carbon"). The graphite wire was evaporated using a current pulse. The current pulse and resulting evaporation time was estimated as less than one second. The MLM sample was placed on a copper mount, facing the wire at a distance of 5-10 cm. The short duration of the current pulse and the copper mount ensure the temperature of the mirror does not change significantly over the duration of the exposure.

2.2 Spectroscopy ellipsometry

Ellipsometry measures the change in polarization state of light beam reflected from the surface of a sample. Generally, the change in polarization is expressed by two ellipsometric angles, i.e. psi (Ψ) and delta (Δ), which is related to the ratio of two Fresnel reflection coefficients r_p and r_s for *p*- and *s*- polarized light, respectively.

$$\frac{r_p}{r_s} = \tan(\Psi)e^{i\Delta} \tag{1}$$

A variable angle spectroscopic ellipsometer (Woollam, VASE) was used to determine the thickness and optical constants of the carbon films, assuming different carbon morphologies. The films were investigated in the photon energy range 0.8-4.5 eV (280-1550 nm), and at incidence angles of 65°, 70° and 75° with respect to the surface normal. A single scan takes about 10 minutes, but this can be substantially reduced by using more sophisticated detectors.

#111052 - $15.00 USD Received 6 May 2009; revised 7 Sep 2009; accepted 7 Sep 2009; published 9 Sep 2009
(C) 2009 OSA

The directly measured parameters, Ψ and Δ, do not directly yield the quantities of interest, such as the film thickness and optical constants. Rather, they are functions of the parameters of interest, which are obtained by fitting the measured Ψ and Δ to an optical model. The parameters of interest can then be obtained from a regression analysis.

2.3 Laser generated surface acoustic waves

The LG-SAW experimental setup (see Fig. 1) and operating parameters are described elsewhere [18]. In short, the surface acoustic wave dispersion was determined by the propagation characteristics of a short acoustic pulse. The experimental dispersion curves were used to determine the mechanical properties of the MLM and the carbon film by fitting a theoretical dispersion curve to the measured curve by varying the related parameters, such as Young's modulus, density, Poisson's ratio, and thickness. The number of parameters that can be independently determined depends on the film thickness and the difference between the mechanical properties of the film and the substrate. Note that the degree of nonlinearity of the SAW dispersion curve is crucial for determining the number of parameters that can be independently resolved [14].

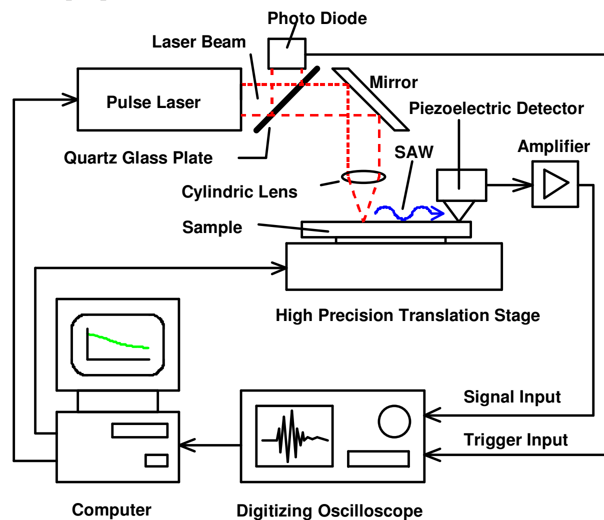

Fig. 1. The system diagram of LG-SAW experimental setup

3. Results of SE

3.1 MLM

The multilayer structure of a mirror is quite complex as it contains more than 100 layers, each several nanometers thick. In addition, the optical properties of the multilayer itself and interfacial layers are still not very well known in the 0.8-4.5 eV photon energy range. In order to extract the thickness and optical constants of the carbon film, the uncontaminated MLM was first characterized. We used an effective dielectric function to describe the optical properties of the MLM. The effective dielectric function simplifies the optical model of the MLM, including a storage related contamination layer, by modeling it as a single "pseudo substrate". The optical constants of the pseudo substrate were obtained from a direct inversion (i.e. it is assumed to be a bulk substrate) of the ellipsometric parameters. Figure 2 shows the resulting effective dielectric function of the MLM. It was assumed that the optical constants of the pseudo substrate, including the storage related contamination layer, do not vary significantly during EUV illumination. It is also observed that all mirrors with the same deposition conditions, even mirrors that are manufactured at different times, have the same optical properties, based on the Ψ and Δ data.

#111052 - $15.00 USD Received 6 May 2009; revised 7 Sep 2009; accepted 7 Sep 2009; published 9 Sep 2009
(C) 2009 OSA

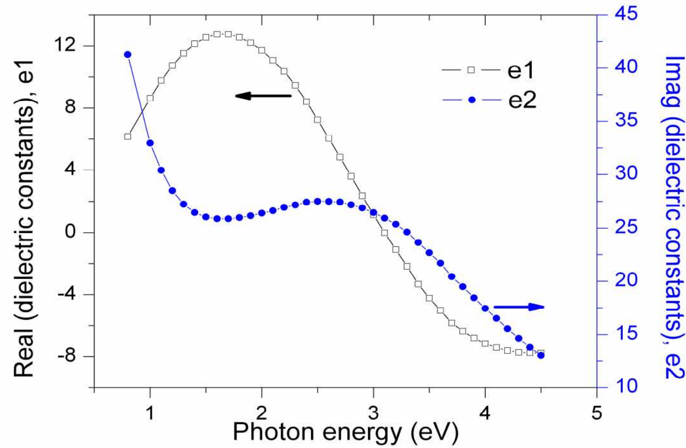

Fig. 2. The effective optical constants of a MLM

The analysis of the carbon contamination layer is done via a standard three-phase model. In this model, the optical properties of two of the phases: the pseudo substrate, and ambient air are set to pre-determined values. The thickness and optical properties of the third phase, which is the contamination layer, are varied to obtain a good fit to the measured Ψ and Δ data.

3.2 Dielectric model of the carbon layers

To interpret the experiment results presented in Fig. 3, a suitable optical model must be chosen. X-ray Photoelectron Spectroscopy (XPS) measurements (data not shown) revealed that the contamination due to EUV illumination is dominated by carbon. But since XPS cannot detect hydrogen and it is very difficult to determine the nature of the carbon layer. On the other hand, LG-SAW results, presented in section 4.2, indicate that the layer is mechanically soft (Young's modulus < 100 GPa) and polymer-like. These results lead us to conclude that the layer is probably a partially hydrogenated amorphous carbon layer. This is supported by the findings of Hollenshead *et al.* who found that surface contamination during EUV illumination consists of a partially hydrogenated amorphous carbon layer [2].

Jellison and Modine have developed a Tauc-Lorentz (TL) model to describe the optical properties of amorphous semiconductors and insulators in the interband region [19,20]. This model has been broadly applied to characterize a-C and a-C:H films [21–24]. We will also use this model to describe the properties of the EUV induced contamination layer. In the TL model, the combination of the Tauc joint density of states [25] and the quantum mechanical Lorentz oscillator have been used to describe the imaginary part of the dielectric function $e2$ as:

$$e2(E) = \left[\frac{A E_0 C (E - E_g)^2}{\left(E^2 - E_0{}^2\right)^2 + C^2 E^2} \cdot \frac{1}{E} \right] \quad \text{for } E > E_g \tag{2}$$

$$e2(E) = 0 \quad \text{for } E <= E_g \tag{3}$$

where A (the amplitude), E_0 (the peak transition energy), E_g (the optical band gap) and C (the broadening term) are four fitting parameters with units of energy, while E is the photon energy. The corresponding real part of the dielectric function can be found from the Kramers-Kronig relationship. The band gap is used as a cutoff energy so that photons with energy less than E_g suffer no absorption.

The films obtained by hot filament carbon evaporation are not expected to have significant hydrogen content. Additionally, the deposition conditions are inconsistent with those that deposit diamond-like carbon films. Furthermore, the LG-SAW results, presented in section

#111052 - $15.00 USD Received 6 May 2009; revised 7 Sep 2009; accepted 7 Sep 2009; published 9 Sep 2009
(C) 2009 OSA

4.2, show that the Young's modulus is about 370 GPa, which is in the general range of amorphous carbon films. The Tanguy model [26–28] was recently developed to provide an analytical expression of dielectric constants of Wannier excitons, including bound and unbound states. It has been introduced to describe the optical properties of gallium arsenide [29]. Here, we also use Tanguy model for the hot filament carbon films.

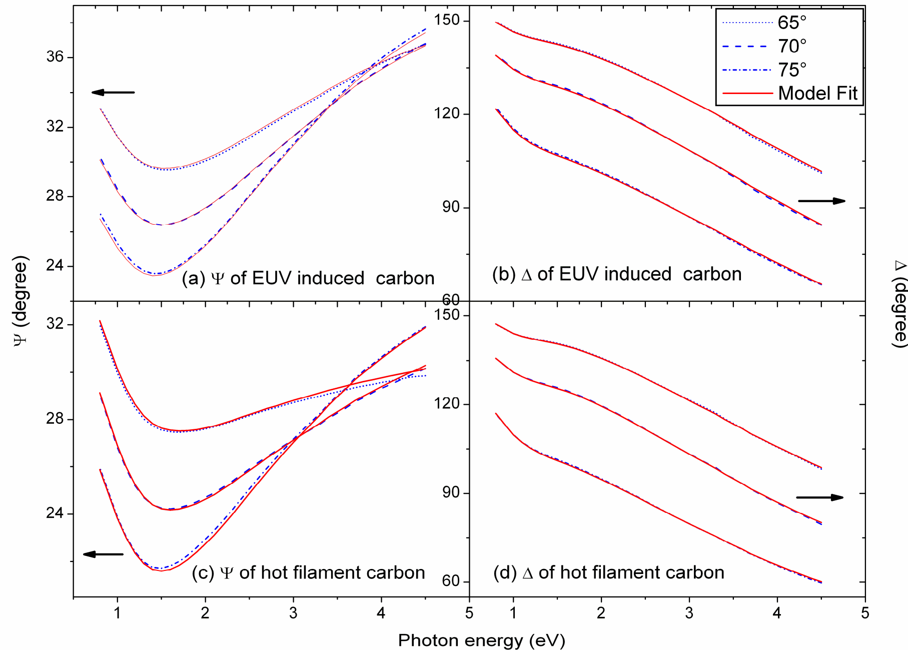

Fig. 3. The fitting of ellipsometric angles Ψ and Δ for the MLM deposited by 23.2 nm EUV induced carbon and 11.9 nm hot filament carbon.

3.3 Fitting results

The fitting results are shown in Fig. 3. A good fit, with a mean-squared error (MSE) < 1 is obtained for both EUV induced carbon and hot filament carbon films. The optical properties of EUV induced carbon were determined from the MLM exposed to the most EUV illumination (5 Mega pulses). These parameters were then held fixed for all other EUV induced carbon films, leaving only the layer thickness as a free parameter. All of the fitting resulted in MSE < 1, indicating that the optical properties of the thinner layers are quite similar to the thickest layer. A simultaneous fit of thickness and optical properties for the very thin layers would show too large a dependence between fit parameters and therefore large inaccuracies of the fit results. The dielectric function of EUV induced carbon films are shown in Fig. 4 (a). The film is almost transparent throughout the visible and near infrared region, as expected for polymer-like hydrocarbon and diamond-like carbon. However, the real part of dielectric function is less than the value generally reported for diamond-like carbon and is similar to polymer-like hydrocarbon (e.g. polypropylene) [23].

A similar procedure was used for the hot filament carbon films. As can be seen in Fig. 3 (c) and (d), a good fit is obtained for the film of 11.9 nm. But the error margins of a few parameters in Tanguy model are relatively high. We do not yet fully understand why these parameters are less tightly constrained by the fitting process, or if these errors mean that a more suitable model could be found. However, the resulting thicknesses are comparable to results obtained using X-ray diffraction analysis. The dielectric function of the hot filament carbon film is also shown in Fig. 4 (b). The strong broad absorption in the visible region is clearly visible, confirming the general amorphous carbon nature of the film.

SE can clearly distinguish between these two carbon films, indicating that it should be possible to determine the hydrogen content of the films from their optical properties. However, this requires a hydrogen sensitive technique to provide independent calibration, which is beyond the scope of this work.

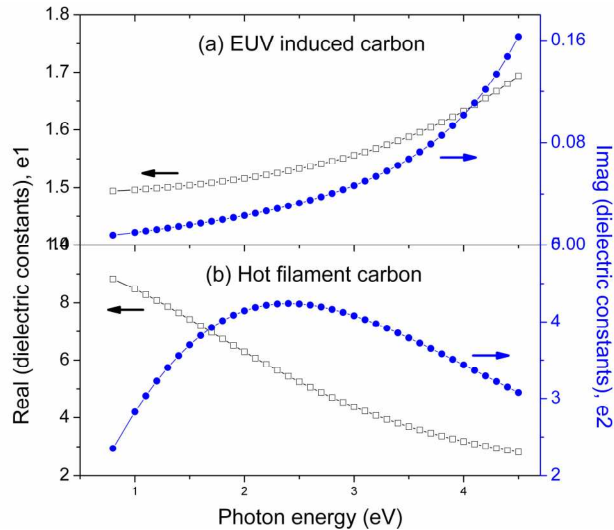

Fig. 4. The dielectric constants of hot filament carbon film (a) and EUV induced carbon contamination film (b).

3.4 The limit of detection

The limit of detection has been investigated for EUV induced carbon films in order to check the feasibility for sub-nanometer in situ carbon contamination monitoring for EUV optics. Figure 5 plots ellipsometric angles Ψ and Δ as a function of thickness at 4 eV and 75°. The sensitivity of Ψ and Δ for thicknesses up to 1.5 nm is 0.4 and 1.9 degree per nanometer, respectively. The uncertainty of individual Ψ and Δ measurements are about 0.3 and 0.7 degrees, respectively.

The uncertainty in the thickness of the EUV induced carbon layer has two sources: the uncertainty of its optical constants, and the measurement uncertainty of Ψ and Δ. The uncertainty due to the optical constants is a systematic uncertainty because they are not independently measured. However, these uncertainties are unlikely to be significant because the measured thicknesses for different EUV induced carbon samples are consistent with the changes in illumination time.

In our case, the uncertainty of an individual thickness measurement is less than 0.1 nm. The limit of detection, calculated as three times of the standard deviation (with the optical constants held fixed), is about 0.2 nm. Note that a state-of-the-art ellipsometer has an order of magnitude less uncertainty in Ψ and Δ, so we can expect that the detection limit can be reduced to sub-monolayer thicknesses.

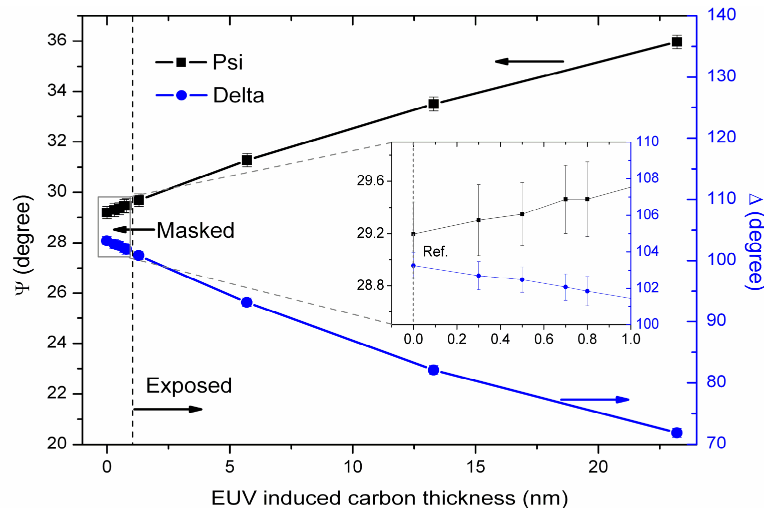

Fig. 5. Ellipsometric angles psi and delta as a function of EUV induced carbon thickness at 4 eV and 75° with an expanded section shown in the inset figure.

4. Results of LG-SAW

4.1 MLM

LG-SAW measurements were performed on both the exposed and masked sections of the MLM samples under EUV illumination. In general, SAW pulses with a frequency bandwidth up to 220 MHz were generated and detected. Taking into account the well defined layer thicknesses for the MLM, and using the average value of Possion's ratios of Mo and Si, and average densities that are 85% of the bulk value [30], we find that the effective Young's modulus for the MLM is 168 GPa.

4.2 Dispersion curves fitting

To characterize the properties of the carbon layer on the MLM, the carbon layer's contribution to the SAW dispersion must be separated from the dispersion of the underlying MLM. An approach to achieving this separation is to subtract the dispersion curve due to the unexposed section of the MLM from the dispersion curve obtained from the exposed section. This corrected dispersion curve is then used to characterized the properties of the carbon layer. The dispersion curves obtained from the MLMs with EUV induced carbon and hot filament carbon are shown and analyzed in reference [18] in detail. For EUV induced carbon layers with thicknesses of 5 and 22.5 nm (corrected by the masked part of the MLM), the slope of corrected dispersion curve is quite close to zero, though still negative, indicating that the Young's modulus of EUV induced carbon is smaller than that of the Si wafer (169 GPa). Young's modulus was found to increase with thickness from 17 ± 11 GPa for a 5 nm thick carbon layer to 41 ± 9 GPa for a 22.5 nm thick films. It is typical to find that Young's modulus increases with film thickness for layers only a few nanometers thick.

A similar analysis was performed on MLMs that had hot filament carbon layers deposited on them. The corrected dispersion curve is also linear, but with a positive slope, clearly showing anomalous dispersion. This indicates that it has a Young's modulus larger than that of the underlying silicon substrate. By fitting the corrected dispersion curve, Young's modulus was found to be 371 ± 9 GPa and 373 ± 1 GPa for the 11.9 nm for 24.3 nm thick films, respectively. This small difference is expected since the deposition time is very short and the MLM surface temperature was kept at nearly room temperature, leaving little chance for annealing. In contrast, EUV induced carbon is subject to constant bombardment by ~90 eV photons and lower energy photoelectrons during an illumination that lasts for 2-5 hours.

#111052 - $15.00 USD Received 6 May 2009; revised 7 Sep 2009; accepted 7 Sep 2009; published 9 Sep 2009
(C) 2009 OSA

4.3 The limit of detection

Based on the measurements on EUV induced carbon films on top of MLMs [18], the uncertainty of SAW dispersion curve is about 0.1 m/s. Since the dispersion curve is linear, a value for the layer thickness can only be obtained if the density, Young's modulus and Poisson's ratio are known. In general, these parameters are not well known for EUV induced carbon films, and consequently, contribute greatly to the uncertainty of the measurement.

Aside from these considerations, it should be noted that detection is not the same as characterization, where, for detection, we require that the dispersion curve is detectably different from a reference curve. LG-SAW was found to be sensitive enough to characterize a EUV induced carbon layer with a thickness of 5 nm on top of a MLM. So the detection limit is somewhat less than 5 nm. The calculation of the limit of detection is complicated by the fitting procedure, however, it can be estimated from the uncertainty of dispersion curve slope. The standard deviation of slope fitting of 10 measurements on the same location is 5.1×10^{-4} $ms^{-1}MHz^{-1}$. In contrast, the slope observed for the 5 nm thick layer is 4.4×10^{-3} $ms^{-1}MHz^{-1}$. This leads to an estimate of 2 nm for the limit of detection for EUV induced carbon layers on a MLM.

On the other hand, LG-SAW can discriminate these two different carbon films based on their acoustic properties, i.e. the absolute speed of SAW. The SAW phase velocity of EUV induced carbon is less than the propagation velocity of about 5081 m/s in the [110] direction on a clean (001) silicon wafer. But for hot filament carbon, the phase velocity is larger than that of the silicon wafer.

5. Discussion and conclusion

To place our results in a wider context, we measured the EUV reflectance for these carbon contaminated MLMs with a reflectometer at the radiometry laboratory of the Physikalisch-Technische Bundesanstalt (PTB) at the BESSY II electron storage ring [31]. This enabled us to measure the absolute reflectance with a relative uncertainty of 0.25%. Figure 6 shows the loss of the maximum reflectance as a function of carbon growth for both hot filament and EUV induced carbon. It shows that the reflectance loss of hot filament carbon is larger than the EUV induced carbon with the same thickness. The relative reflectance loss is 1.1% (i.e. absolute loss 0.7%, ~three times the measurement uncertainty) when a MLM has a 1.3 nm thick layer of EUV induced carbon on top of it. In contrast, Hollenshead and Klebanoff [2] claimed that the projection optics of an EUVL tool should not lose more than 1.6% reflectance per optic. Thus, ellipsometry would be sensitive enough for contamination monitoring. In addition, sub-monolayer detection is achievable with a state-of-the-art ellipsometer. As noted in the introduction, SE is non-contact, non-destructive and fast if advanced CCD detection applied, making it a good candidate for contamination monitoring. On the other hand, as our results show, it can be difficult to choose the best model from which physical parameters are derived. This makes it critical to understand contamination mechanisms and what form of carbon is likely to form over a range of EUVL operating.

LG-SAW is relatively simpler to set up and the data interpretation is easier than for SE. However, it is not as sensitive or as fast as SE. It is also, currently, a contact technique, in which a piezoelectric detector has to be fixed on top of the sample. In addition, the LG-SAW measurement methodology makes contamination mapping not straightforward. More importantly, according to the specifications of the piezoelectric detector we used, it will not work properly at temperatures higher than 100 °C, which could be a limitation for some optics.

One limitation of using LG-SAW is the substrate requirement. In order to generate and detect SAW at high frequencies (about 200 MHz), the substrate must be crystalline to have a sufficiently low absorption. This requirement may not be met for some optics. In addition, the difference between dispersion curves from different MLM references is about 1.6 m/s at 200 MHz, due to differences between different MLM and substrates. This velocity difference is

#111052 - $15.00 USD Received 6 May 2009; revised 7 Sep 2009; accepted 7 Sep 2009; published 9 Sep 2009
(C) 2009 OSA

larger than the velocity change due to 5 nm of EUV induced carbon, meaning that reference dispersion curves for individual MLMs must be obtained.

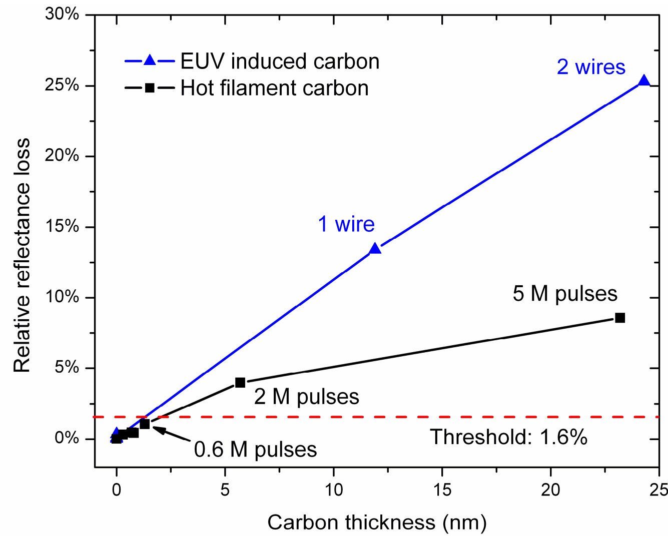

Fig. 6. Absolute EUV reflectance loss as a function of carbon thickness. The blue curve is hot filament carbon with two different thicknesses by evaporating 1 and 2 wires of graphite. The black curve is EUV induced carbon growth with three different amounts of EUV pulses, 0.6, 2 and 5 mega pulses.

Acknowledgements

This research was carried out under the project number MC3.06245 in the framework of the Research Program of the Materials Innovation Institute M2i (www.m2i.nl, the former Netherlands Institute for Metals Research), the "Stichting voor Fundamenteel Onderzoek der Materie FOM," the latter being financially supported by the "Nederlandse Organisatie voor Wetenschappelijk Onderzoek NWO" and SenterNovem through the "ACHieVE" programme. We gratefully acknowledge Wilfred van der Wiel at University of Twente, Paulo V. Santos at the Paul Drude Institute for Solid State Electronics, S. Vikram Singh and M. C. M. van de Sanden at the University of Technology Eindhoven for useful discussion and information. Eric Louis and Fred Bijkerk acknowledge support by the FOM Industrial Partnership Programme I10 ('eXtreme UV Multilayer Optics'), co-funded by the Foundation FOM and Carl Zeiss SMT AG.

#111052 - $15.00 USD Received 6 May 2009; revised 7 Sep 2009; accepted 7 Sep 2009; published 9 Sep 2009

(C) 2009 OSA